Rend. Fis. Acc. Lincei (2016) 27 (Suppl 1):S47–S58
DOI 10.1007/s12210-016-0529-3

ENVIRONMENTAL CHANGES IN ARCTIC

Size distribution and ion composition of aerosol collected at Ny-Ålesund in the spring–summer field campaign 2013

F. Giardi[1] · S. Becagli[1] · R. Traversi[1] · D. Frosini[1] · M. Severi[1] · L. Caiazzo[1] · C. Ancillotti[1] · D. Cappelletti[2] · B. Moroni[2] · M. Grotti[3] · A. Bazzano[3] · A. Lupi[4] · M. Mazzola[4] · V. Vitale[4] · O. Abollino[5] · L. Ferrero[6] · E. Bolzacchini[6] · A. Viola[7] · R. Udisti[1,4]

Received: 27 November 2015 / Accepted: 19 April 2016 / Published online: 9 May 2016

Abstract During the 2013 Arctic campaign, direct measurements and size-segregated samplings of atmospheric aerosol were carried out from March to September at the Gruvebadet observatory in Ny-Ålesund (78°56′N, 11°56′E; Svalbard Islands). Continuous size distribution measurements (104 size classes) were performed both in the nano- (TSI-SMPS system) and micro-metric (TSI-APS device) range with a resolution of 10 min. Aerosol sampling was carried out on daily basis (PM_{10} fraction, 00:01–23:59 UTC) and with a 4-day resolution (four-stage cascade impactor). A back-trajectory analysis was performed for specific events to understand transport processes and possible source areas of aerosol reaching Ny-Ålesund. Aerosol samples were analyzed for ion composition (inorganic cations and anions, selected organic anions) by a three-chromatograph system after extraction in ultra-sonic bath. Special attention was spent in identifying and interpreting the seasonal pattern of natural and anthropic chemical markers. Sea spray aerosol was evenly distributed along all the sampling period with maxima related to wind speed. Its size distribution peaks in 1.0–2.5 or 2.5–10 μm, depending on the transport conditions and distance from source areas. Anthropic sulfate dominates the spring aerosol load (Arctic Haze), both in acidic form (H_2SO_4) and in partially or totally neutralized ammonium salts. Biogenic contributions, marked by methanesulfonic acid, are relatively relevant in late spring–early summer and are distributed in the finest aerosol fraction (<1.0 μm).

Keywords Aerosol · Arctic · Ion chromatography · PM10 · Size distribution

This peer-reviewed article is a result of the multi and interdisciplinary research activities based at the Arctic Station "Dirigibile Italia", coordinated by the "Dipartimento Scienze del Sistema Terra e Tecnologie per l'Ambiente" of the National Research Council of Italy.

✉ F. Giardi
fabio.giardi@unifi.it

[1] Department of Chemistry "Ugo Schiff", University of Florence, Sesto Fiorentino, 50019 Florence, Italy

[2] Department of Chemistry, University of Perugia, 06100 Perugia, Italy

[3] Department of Chemistry and Industrial Chemistry, University of Genoa, 16146 Genoa, Italy

[4] CNR-ISAC, 40129 Bologna, Italy

[5] Department of Chemistry, University of Turin, 10125 Turin, Italy

[6] Department of Environmental Sciences, University of Milano-Bicocca, 20126 Milan, Italy

[7] CNR-ISAC, 00133 Rome, Italy

1 Introduction

The Arctic is one of the most sensitive environments to climate perturbations. The arctic mean surface temperature in the last decades has been observed to increase faster than the mean global average (IPCC 2013). This phenomenon, known as *Arctic Amplification*, is the result of complex feedback mechanisms, such as the decrease of sea ice extent which influences the global radiative balance by reducing the surface albedo. The consequent positive feedback leads to a more rapid sea ice loss (Robock 1983; Screen and Simmonds 2010).

Particulate matter plays an important role within the global climate system and then again in the Arctic. Suspended particles can perturb the radiative balance both through their direct effects of scattering and absorption

mechanisms of the solar radiation (IPCC 2013), which are the functions of aerosol's size distribution, concentration, and chemical composition. These characteristics have a large variability along the year and depend on aerosol sources and transport processes. Aerosol also has an indirect effect in the interaction with solar radiation, it concerns the modification of cloud microphysics affecting cloud albedo and lifetime (Albrecht 1989; Pincus and Baker 1994). Aerosol particles can act as Cloud Condensation Nuclei (CCN), leading to the formation of a larger number of water droplets that increase the reflectivity of clouds. The ultimate magnitude of the aerosol relative forcing depends on the weight of direct and indirect effects. Thus, to reduce the uncertainty about this climate-forcing factor and to better understand the influence of human contribution, it is particularly relevant to study the current aerosol features in the Arctic in terms of atmospheric load and chemical composition in the different size classes.

The impact of aerosol in the Arctic has proved to be highly variable during the year. The most important contribution to the Arctic particulate matter occurs in the winter–spring period because of a phenomenon known as *Arctic Haze* (Quinn et al. 2007). This tropospheric brown haze mainly consists of high concentrations of sulfates, organic compounds, and other trace elements (Heintzenberg et al. 1981), which principally spread in the accumulation mode (Shaw 1984), as expected for the secondary aerosol especially related to anthropic sources (Bazzano et al. 2016). These particles, once transported northward from mid-latitude industrialized areas, end up in the cold and stable atmosphere, which inhibits turbulent transfers between different layers as well as the formation of clouds and precipitations, which are the major particulate matter removal ways (Iversen and Jorenger 1985). The combination of these factors results in the transport of aerosol particles to the Arctic and the trapping of the pollutants in a phenomenon that usually lasts until the end of April. Other aerosol sources, such as biogenic emission and on-site particle formation, dominate summer aerosol (Leck and Persson 1996).

As a consequence of this source shift, Arctic aerosol showed pronounced seasonal variations in the size distribution, with sudden changes in the chemical and physical properties between late winter–spring and summer periods above the planetary boundary layer (Ström et al. 2003; Engvall et al. 2007; Tunved et al. 2013). In this work, some relevant results of a spring–summer campaign of ground-based aerosol sampling are discussed to identify the different sources of the arctic aerosol from chemical composition and size distribution measurements.

2 Methods

2.1 Sampling

The Arctic aerosol samples were collected at Gruvebadet, the Italian observatory in Ny-Ålesund (78°56′N, 11°56′E, Svalbard Islands, Norway) in 2013, during the spring and summer seasons. The observatory is located about 1 km south-east of the village in a clean area, where every motorized activity was forbidden. Pumps were installed inside an insulated room, and the sampling heads were placed on the roof of the building. External temperature probes allow to maintain the air flow stable at actual conditions, namely, the temperature and pressure conditions recorded outside; this is basic to not compromise the wanted cut-off value, which would change in the case of room temperature normalized volumes.

The aerosol analyzed in this work was collected by two devices. The first was a Tecora Skypost PM, a low-volume sampler (38.33 L min^{-1}) which allowed to automatically collect the daily samples of particulate matter (00:01–23:59 UTC) with aerodynamic equivalent diameter (AED) smaller than 10 μm. Aerosol particles were collected on Teflon filters (47 mm diameter, 2 μm nominal porosity, and capture efficiency of 99.6 % for 0.3 μm particles). The second data set was obtained by a four-stage Dekati PM_{10} multi-stage impactor (29.00 L min^{-1}, 4-day resolution, and cascade impactor). Polycarbonate filters (25 mm diameter and 0.1 μm nominal porosity) were used as substrate for the first three stages (AED >10 μm, 10–2.5 μm, and 2.5–1.0 μm), while a Teflon filter collected the sub-micrometric particles (AED <1.0 μm) in the last stage. The total number of samplings collected during the campaign was 165 for PM_{10} and 41 for the four stages. The sampling period and the number of samples for each year are reported in Table 1. Exposed filters were stored at −20 °C in sealed plastic bags, until analysis.

Size distribution data were evaluated by two particle counters: TSI SMPS, 54 channels (32 ch./decade), to detect nanometric particles with electrical mobility diameter between 10 and 487 nm and TSI APS, 52 channels (32 ch./decade), for the micrometric particles, in the aerodynamic equivalent diameter range 0.523–20.536 μm. Size distribution measurements were continuously carried out at a 10-min resolution in the period between April 6th and September 15th (99.8 % time coverage).

2.2 Chemical analysis

Before and after exposure, each PM_{10} Teflon filter was weighed; and, using the actual sampled volumes, the atmospheric concentration of particulate matter was

Table 1 Sampling instrumentation settings and samples collected

	PM_{10}	DK4
Impactor	Tecora (10 μm cut-off)	Dekati PM_{10} (multistage)
Pump device	Tecora Skypost PM	Tecora Echo PM
Flow (actual conditions)	38.33 L min^{-1}	29.00 L min^{-1}
Resolution (h)	24	96
Filters/substrate	Teflon (Pall Corp.), Ø 47 mm, 2 μm porosity, efficiency 99.6 %	Teflon (Pall Corp.); Polycarbonate (Whatman), Ø 25 mm, 0.1 μm porosity
Size classes (support)	<10 μm	>10 μm (PC); 10–2.5 μm (PC); 2.5–1.0 μm (PC); <1.0 μm (Teflon)
Sampling period	31 Mar 13–14 Sep 13	31 Mar 13–10 Sep 13
Samples number	165	41

PC polycarbonate, *Teflon* polytetrafluoroethylene

calculated. At the time of analysis, to avoid contamination, samples were handled inside a clean room (class 10,000), under a laminar flow hood (class 100), using powder-free gloves. The soluble components present in each sample were extracted from half-filter in about 12 ml of ultrapure water (MilliQ, 18 MΩ cm, exactly determined by weighing) in ultrasonic bath for 15 min. Analysis was performed using a three IC-system (Dionex), respectively, setup for the determination of cations (Na^+, NH_4^+, K^+, Mg^{2+}, and Ca^{2+}), inorganic anions (F^-, Cl^-, NO_2^-, Br^-, NO_3^-, and SO_4^{2-}), and selected organic anions (acetate, glycolate, propionate, formate, methanesulfonate, pyruvate, and $C_2O_4^{2-}$). Ion chromatographic conditions are reported in Table 2, while detection limits and blank values of the main ion species are reported in Table 3.

2.3 Trajectories calculation

Backward trajectories at 500 m a.s.l. were generated using the vertical velocity option of the Hybrid Single-Particle Lagrangian Integrated Trajectory (HYSPLIT) model (Stein et al. 2015).

3 Results and discussion

High temporal resolution for the total PM_{10} and four-stage impactor data was tested for internal consistency. For each component, the comparison was made between the concentration of PM_{10} samples (averaged over 4 days) and the sum of the concentration measured in the 10–2.5 μm, 2.5–1.0 μm, and <1.0 μm stages. Despite the difference between the two sampling devices (efficiency and size separation system), a close similarity in concentration levels was observed along the whole time period for almost all the species, with a discrepancy lower than 16 % for the main species (Table 4), that is justified by the uncertainty of the slope and the analytical method. Larger differences were found for species present in the samples at very low concentrations, likely because of larger uncertainties in evaluating blank values in the four-stage samples.

The atmospheric concentration of daily PM_{10} showed that most of the particulate matter ionic composition (over 95 %) was represented by Cl^- (30.5 %), SO_4^{2-} (26.5 %), Na^+ (23.1 %), NH_4^+ (5.8 %), Mg^{2+} (2.8 %), NO_3^- (2.7 %), MSA (2.4 %), and Ca^{2+} (1.9 %), whereas the others (each one accounting for much less than 2 % of the total PM_{10} budget) composed the remaining 4.3 %.

3.1 Size distribution

The availability of a large number of channels (104), joined with the high temporal resolution (10 min), allowed appreciating fast changes in atmospheric particle population. In the two 2D color plots reported in Fig. 1, the particle counts for each instrument in April 6–15 September, 2014 period are shown. The APS plot (Fig. 1a) shows the highest particle concentration in the 0.5–1.0 μm range in spring.

Starting from the end of April, the submicrometric and micrometric particles decrease down to very low summer values. By taking April 28th as border line, before and after this date, the distribution peaked at 723 nm (diameter midpoint of the size class), but the average concentration of the period after April 28th is 20 times lower (Fig. 2). In the same period, SMPS plot (Fig. 1b) showed an abrupt change in the size distribution. In the first period, particles peaked at 184 nm and their atmospheric concentration was relatively constant ($dN/dlogD_p$ around 10^3). Since late April, the new particle formation (NPF) appears to be the

Table 2 IC-system settings

Detector	Suppressor	Column:	Guard column:	Elution	Sample load	Chromatographer	Ions	
Conductometric CD 20	Electrochemical CSRS-300 4 mm	IonPac CS 12A 4 × 250 mm	IonPac CG 12 4 × 50 mm	Isocratic. Elution: H_2SO_4 22.5 mN, 1.5 mL min^{-1}	Loop 800 µm	Dionex ICS-1000	Na^+, NH_4^+, K^+, Mg^{2+} Ca^{2+}	Cations
		IonPac AS 12A 4 × 250 mm	IonPac AG 4A 4 x 50 mm	Isocratic. Elution: CO_3^{2-} 2.5 mN, 2.0 mL min^{-1}	Preconcentrator IonPac TAC-2 3 × 35 mm, 1,6 mL	Dionex ICS-1000	Cl^-, NO_2^-, Br^-, NO_3^-, SO_4^{2-}, $C_2O_4^{2-}$	Inorganic anions
		IonPac AS11 4 × 250 mm	IonPac AG11 4 × 50 mm	Gradient: $Na_2B_4O_7{\cdot}10\ H_2O$ 1.9 mM and MilliQ water, 1.6 mL min^{-1}	Preconcentrator IonPac TAC-2 3 × 35 mm, 2,2 mL	Dionex DX-500	F^-, acetate, glycolate, propionate, formate, MSA and pyruvate	Organic anions

Table 3 Detection limits and blank values expressed in ng/m^3 for the PM_{10} samples collected on Teflon filters (mean sampling volume = 55 m^3) and for the four-stage samples collected on Teflon filter and PC membrane (mean sampling volume = 155 m^3)

Species	PM_{10} (ng/m^3)		Four-stage (ng/m^3)		
	d.l.	Blank	d.l.	Blank Teflon	Blank PC
Cl^-	0.08	7.88	0.03	2.80	0.04
NO_3^-	0.07	3.11	0.02	1.10	0.03
SO_4^{2-}	0.08	0.74	0.03	0.26	0.18
MSA	0.01	d.l.	<0.01	d.l.	d.l.
Ca^{2+}	0.02	1.39	0.01	0.49	0.02
Mg^{2+}	0.04	0.20	0.02	0.07	0.01
Na^+	0.04	6.24	0.01	2.21	0.26
NH_4^+	0.09	0.07	0.03	0.03	0.09

dominant mode of the atmospheric aerosol, with short and well-characterized (banana shaped) NPF events. The previous study carried out at Zeppelin (Ny-Ålesund) showed that new particle formation events seem to be a rather common phenomenon during the Arctic summer, and this is the result of both the photochemical production of nucleating/condensing species and low condensation sink (Tunved et al. 2013). Based on the visual analysis described by Dal Maso et al. (2005), during the sampling period (163 days), 50 clear NPF events were identified starting from the end of April. Besides, in many cases, the nucleation started under the lower size class of the instrument (10 nm); on average, the particles grew up to 20–40 nm. Since in springtime and summertime, the sun is always present; during the day, the particle formations did not have a preferential time of the day to begin, whereas the events have lasted for 2–24 h.

This seasonal pattern of NPF events can be interpreted as follows: during March–April, there is sunlight but also a large preexisting surface due to the presence of long-range transported aerosol (mainly sulfate, see Sect. 3.3). The waters are mainly covered by sea ice which means poor conditions for new particle formation as newly formed particles are scavenged quickly, as are any potential nucleating gases (which in any cases likely are produced at a slow speed due to the lack of significant insolation). If the source of the precursor gases is the ocean itself, any emission of such is likely hindered by the ice cover. During May–June, conditions are quite different, and there is more sunlight and less abundant preexisting accumulation mode particles. This allows the newly formed particles to grow into a large enough size that the particle lasts into the following day. These processes happen until August. The summer months are all characterized by high insolation, low aerosol surface (and mass), and a much higher fraction

Table 4 Linear correlation between daily PM_{10} and reconstructed PM_{10} from four-stage samples for the main species; their mean values and mass percentage in the measured soluble fraction in the daily samples and size distribution in the four stages

Species	Linear correl.		PM_{10} mean value (ng/m^3)	% in PM_{10} (solub. part)	Size distribution %			
	Slope	R^2			<1 μm	1–2.5	2.5–10	>10
Cl^-	1.03 (±0.04)	0.94	335.6	30.5	9.5	38.2	42.0	10.3
NO_3^-	0.95 (±0.04)	0.93	29.4	2.7	15.6	53.5	27.6	3.4
SO_4^{2-}	0.92 (±0.03)	0.97	290.8	26.5	82.0	10.2	6.3	1.5
MSA	1.15 (±0.05)	0.94	26.0	2.4	83.5	10.4	4.5	1.6
Ca^{2+}	1.13 (±0.06)	0.89	20.6	1.9	36.7	29.5	25.2	8.6
Mg^{2+}	1.07 (±0.04)	0.95	30.4	2.8	18.7	41.1	32.5	7.7
Na^+	1.16 (±0.03)	0.98	253.7	23.1	17.8	39.9	34.3	8.8
NH_4^+	0.91 (±0.04)	0.94	63.7	5.8	94.0	3.8	1.7	0.6

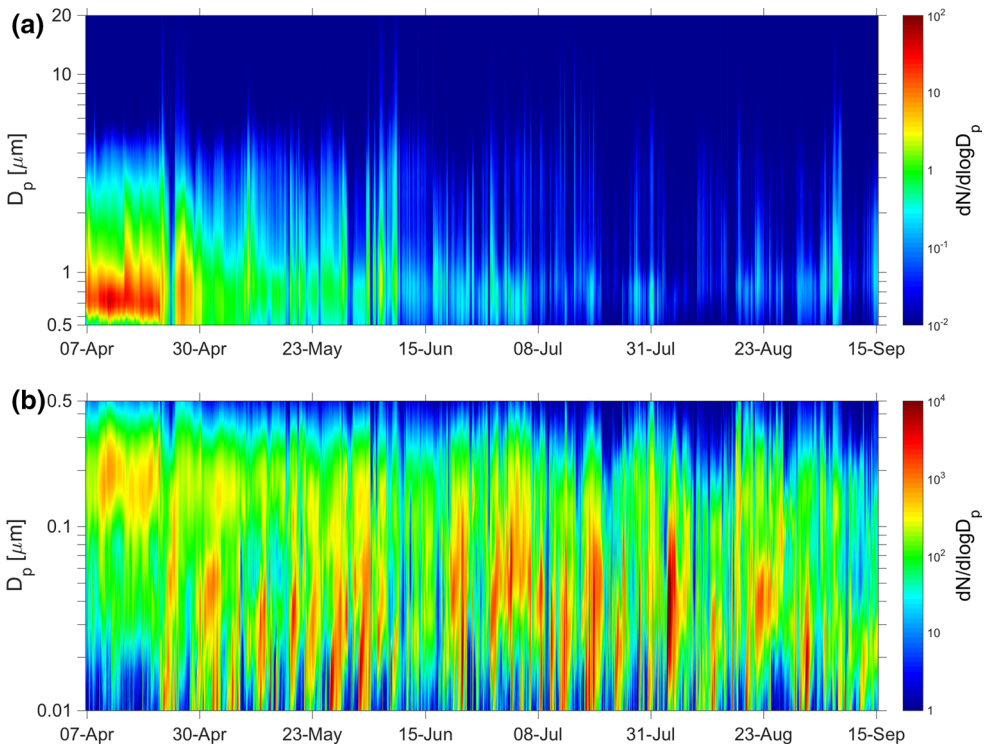

Fig 1 3D color plots from APS (**a**) and SMPS (**b**) particle-counter data, showing the aerosol size distribution along the whole 2013 campaign. The number of particles (expressed as $dN/dlogD_p$) is plotted as a function of their mobility diameter for SMPS and aerodynamic equivalent diameter (a.e.d.) for APS

of open ocean. In September, as days become shorter and solar radiation decreases, the particle production ceases and the period of dominating accumulation mode is going to be re-established.

This again indicates the importance of photochemical production as the main driver for new particle formation in the Arctic environment rather than sea salt aerosol. Indeed, a comparison among sea salt aerosol content with new particle formation events showed no correlation between nucleation and daily marine primary emission.

3.2 Sea salt

Sodium, chloride, and magnesium are the main components of the sea spray source, whereas minor contributions are represented by potassium, calcium, and sulfate. Since all these components have other sources than seawater, their sea-spray (ss-) fractions were calculated using $ssNa^+$ as specific marker and knowing the $X/ssNa^+$ weight/weight (w/w) ratios in seawater of each X component (Kulshrestha et al. 1996; Das et al. 2005): 0.036 for K^+, 0.129 for Mg^{2+},

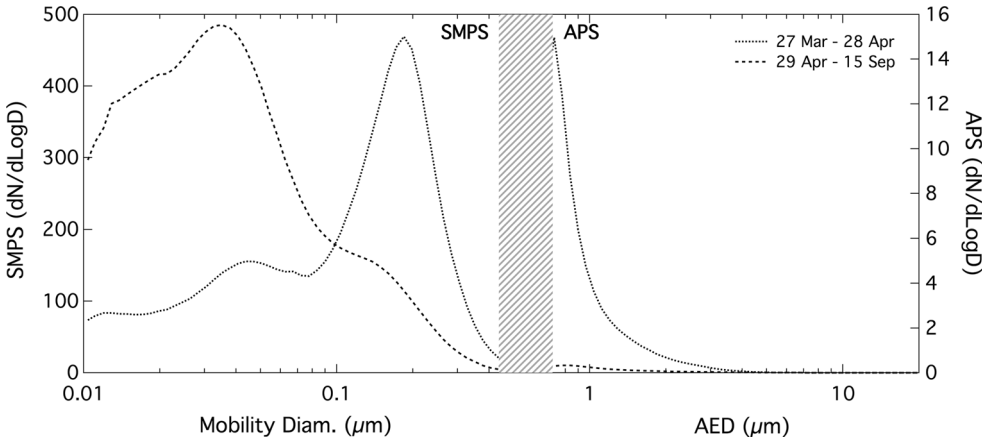

Fig. 2 Average size distribution in two different periods; *dashed area* represents the uncovered gap between the SMPS's *upper* channel and the APS's *lower* one in addition to the low-efficiency channels of APS

0.038 for Ca^{2+}, 1.81 for Cl^{-}, and 0.253 for SO_4^{2-} (Henderson and Henderson, 2009). The nonsea salt (nss-) fraction of every component was evaluated as the difference from its total concentration in the aerosol and the sea salt contribute. A four-variable, four-equation system (Röthlisberger et al. 2002, Udisti et al. 2012) was used to calculate the ss- and nss- fractions of Na^+ and Ca^{2+}, using the Ca^{2+}/Na^+ w/w ratio in sea water (0.038) and the Na^+/Ca^{2+} w/w ratio in the uppermost Earth crust (0.562) (Bowen 1979).

More than 96 % of the total Na^+, Cl^-, and Mg^{2+} mass in PM_{10} was originated by sea spray; conversely, Ca^{2+}, K^+, and SO_4^{2-} have relevant contributions from other sources, especially crustal aerosol (Ca^{2+}) and anthropic emissions (SO_4^{2-}, K^+) by long-range transport from continental regions (Fisher et al. 2011). Sea salt aerosol was calculated by the sum of the sea salt fraction of Na^+, Mg^{2+}, Ca^{2+}, K^+, SO_4^{2-}, and Cl^-. On average, the sea salt fraction of the water soluble part of PM_{10} accounts for 63.5 and 26.8 % of the total PM_{10} mass.

The multi-stage impactor data showed that the sea spray content, marked by $ssNa^+$, is mainly distributed in the 1.0–2.5 μm fraction (44.2 %), whereas its fractions in the 2.5–10 μm range and in the submicrometric particles were, respectively, 28.3 and 24.3 %; only 3.2 % of $ssNa^+$ was present in the coarse particles (above 10 μm).

The temporal trend of $ssNa^+$ does not show any clear seasonality both in PM_{10} and in the micrometric size-classes by multi-stage impactor (Fig. 3). On the contrary, the temporal profile of the sub-micrometric fraction clearly shows significantly higher concentrations in spring, with respect to relatively low summer values.

The dominance of the submicrometric mode even in the sea-salt particles in spring is consistent with the APS spectra in this season (Fig. 1). Such a pattern could be justified by sea-spray particle settling processes during the atmospheric transport. For the same period, we observed large concentrations of nss-sulfate (see later), coming from continental areas as component of Arctic Haze. It is likely that, during the transport of such air masses, they can be enriched in sea spray along the route over marine sectors.

Differences in sea-spray size distribution along the sampling period (Fig. 3) can be attributed to differences in atmospheric pathways supplying sea salt to Ny-Ålesund. To enlighten specific transport processes, a 72-h back-trajectory analysis was carried out on selected time periods (Fig. 4a–d). For each sample, covering a 4-day sampling period, four 500-m back-trajectory was drawn with arrival at Ny-Ålesund day by day. On April 10, the chemical analysis showed low values of sea salt and a relative large concentration of $ssNa^+$ in the submicrometric range. Three out of four backtrajectories (Fig. 4a) traveled over sea-ice areas and, presumably were not supplied by sea-salt, even if their pathways were at low altitude. In contrast, the air masses arriving to Ny-Ålesund on April 9 (blue line) traveled over open sea areas; in particular, air masses were at sea level for the first day and then at about 1000 m in the following 3 days. In this way, the low concentration of sea spray and the shift of the particle size toward the submicrometric mode (by settling in abrupt altitude change and along the transport) could be explained. On the other hand, the three major sea-spray events, occurred on April 26, June 9, and September 9 (Fig. 3), show that $ssNa^+$ is mainly distributed in the super-micrometric stages (especially in the 1.0–2.5 μm range). The corresponding back trajectories (Fig. 4b–d) revealed that air masses traveled over open-sea areas and at very low altitude at least 2 days before reaching Ny-Ålesund. In this way, air masses were enriched in coarse sea spray particles.

3.3 Sulfuric contribution and influence

The second most important contribution to PM_{10} was represented by sulfate (26.5 %). The ss-sulfate was a minor contribution to sulfate budget. The dominant nss-sulfate fraction can be mainly ascribed to anthropogenic sources

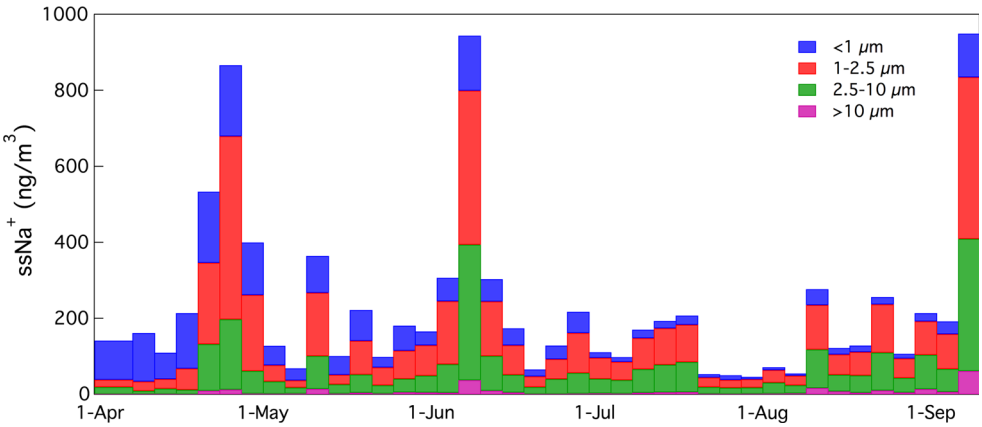

Fig. 3 Temporal profile of $ssNa^+$ in four size classes

(see Udisti et al. 2016), via the atmospheric oxidation of SO_2. Indeed, the temporal profile of $nssSO_4^{2-}$ shows a clear seasonal trend, with maximum values in spring, when Arctic Haze events are more frequent and intense, both in the PM_{10} bulk samples and, especially, in the sub-micrometric fraction (Fig. 5a). In this fraction, sulfate is the most abundant ionic species (65.3 %), followed by ammonium (10.5 %). Indeed, ammonium and oxalate show the same temporal profile of nss-sulfate, with high values in spring and very low summer concentrations. The very similar temporal pattern of ammonium and nss-sulfate highlights the neutralization processes between sulfuric acid and ammonia in the atmosphere. This topic will be discussed in Sect. 3.5.

3.4 Chloride depletion

In the sub-micrometric fraction, the $Cl^-/ssNa^+$ ratio was always lower than the value (1.81 w/w) measured in the seawater (Fig. 5e). This chloride depletion can be attributed to acid–base exchanges between NaCl and acidic species, such as nitric and sulfuric acids, to give sulfate and nitrate salts and gaseous HCl. This reaction, occurring on the sea salt particle surface, is more effective for small particles, with a large surface/volume ratio. Indeed, the mean $Cl^-/ssNa^+$ ratio in the sub-micrometric fraction was 1.07, values significantly lower than those measured in the three super-micrometric stages (from 1.39 to 1.50). Besides, the chloride depletion is expected to be larger in spring, when the atmospheric concentrations of H_2SO_4 in the Arctic haze are higher. Figure 5e shows that the $Cl^-/ssNa^+$ ratio was lower when $nssSO_4^{2-}$ was higher (spring). In late spring–summer period, $Cl^-/ssNa^+$ increases, because the sulfate concentrations are lower and, especially, the dominant sulfate species is $(NH_4)_2SO_4$ and not H_2SO_4 (see Sect. 3.5), so enlightening a lack of free acidity. The exchange reaction between NaCl and acidic species occurs in the atmosphere during the aerosol transport from the ocean to the sampling site, and its effect increases with the residence time of sea spray. In this way, the extent of the chloride depletion is an indicator of the presence of acidic species in the atmosphere, as well as the presence of "aged aerosol", i.e., aerosol formed in regions far from the sampling site and subject to long-range transport processes. To highlight the relevance of the free acidity, 2 days were selected as examples of low and high chloride depletion. Figure 6a shows the 72-h back-trajectory plot for the August 12th PM_{10} sample, where the chloride depletion was little ($Cl^-/ssNa^+ = 1.65$). Back-trajectories at three altitudes show that air masses reaching Ny-Ålesund were coming from North Pole areas, very likely free from anthropogenic contaminants in summer. Indeed, the sub-micrometric record of $nssSO_4^{2-}$ shows very low concentrations in this period (Fig. 5a). Besides, $nssSO_4^{2-}$ is mainly present in neutralized ammonium salts (Fig. 5e). On the contrary, on April 1st, during the spring depletion event, backtrajectories show northward winds delivering air masses from northern Russia (Fig. 6b), likely to deliver sulfate and other acidic species able to cause depletion processes. On this day, the sulfate concentration was quite large (2420 ng/m^3).

3.5 Aerosol acidity

To assess the acidic or alkaline character of the aerosol, ion balances (in nEq/m^3) were evaluated. Since H^+ and HCO_3^{2-} were not directly measured, an excess of anions was counter-balanced by H^+ and an excess of cations by HCO_3^-, as usually accomplished for aerosol and snow from polar areas. Ion balances calculated on the all-period mean values revealed that the super-micrometric fraction was weakly alkaline or neutralized. On the contrary, the sub-micrometric fraction was acidic, probably because of sulfuric acid. Indeed, the temporal profiles of $nssSO_4^{2-}$ and H^+ in the sub-micrometric stage (Fig. 5a, d) are very similar, with the largest free acidity in spring, when the

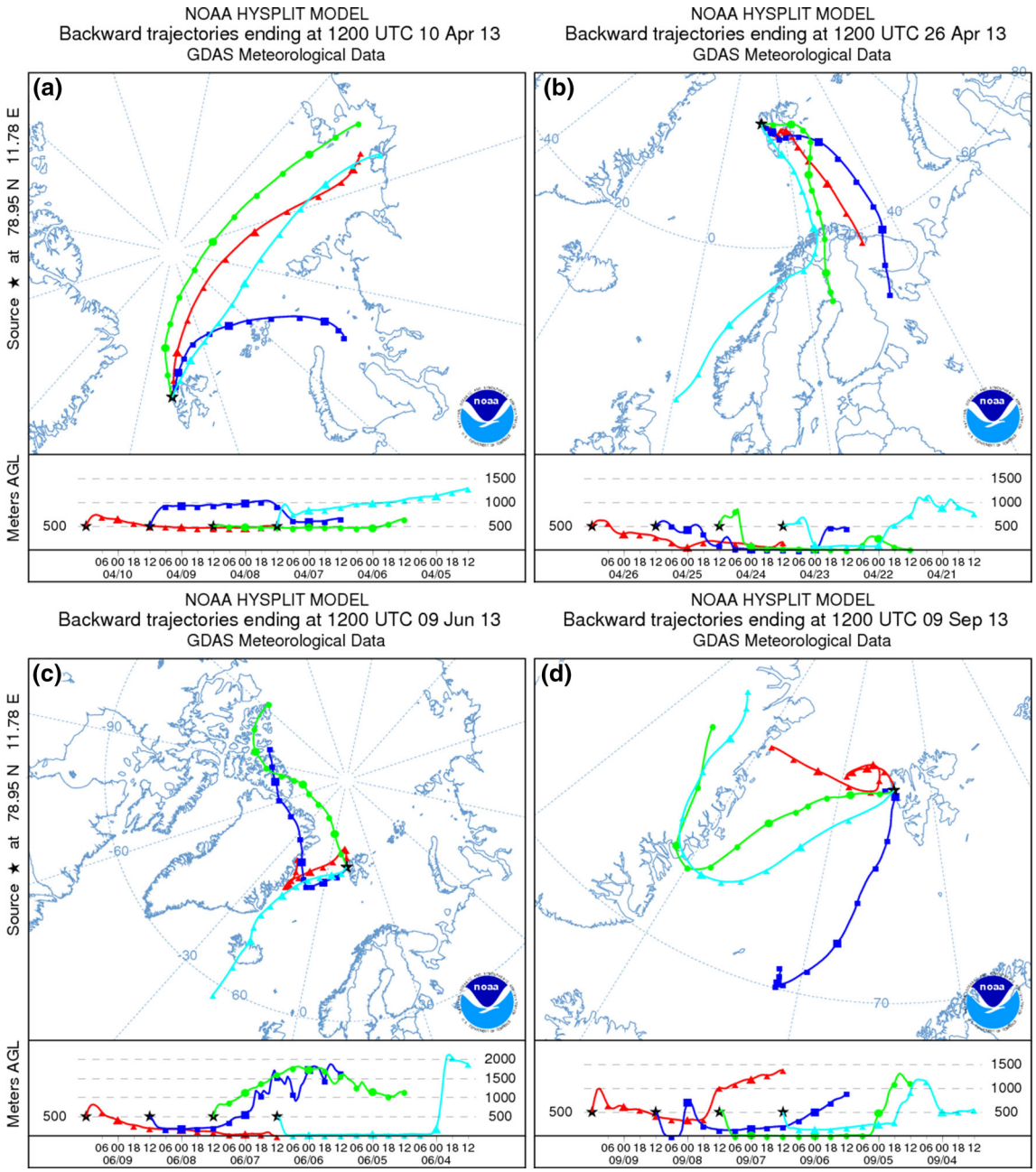

Fig. 4 Backtrajectories (72 h) during events of **a** low and **b–d** high values of sea salt aerosol

highest sulfate concentration was measured. Really, even ammonium shows the highest values in this season (Fig. 5b), but its atmospheric concentrations are not sufficient to neutralize the H_2SO_4 content. Figure 5c shows the temporal profile of the $nssSO_4^{2-}/NH_4^+$ w/w ratio. The values of 2.66 and 5.33 indicate the w/w ratio between the two ions, respectively, in $(NH_4)_2SO_4$ and NH_4HSO_4. In early spring, the SO_4^{2-}/NH_4^+ ratio is higher than 5.33, enlightening the presence of H_2SO_4, i.e., free acidity. From late April to mid-May, the ratio quickly decreases to values around 2.66, showing a progressive neutralization of H_2SO_4 with ammonia to first give NH_4HSO_4 (partial neutralization) and then $(NH_4)_2SO_4$ (complete neutralization). In the late spring–summer period, the sulfate stays completely neutralized (the SO_4^{2-}/NH_4^+ ratio is permanently around the 2.66 value).

3.6 Biogenic emission

Methanesulfonic acid (MSA) is considered as a univocal tracer of marine biogenic activity, because it exclusively results from the atmospheric photo-oxidation (both in

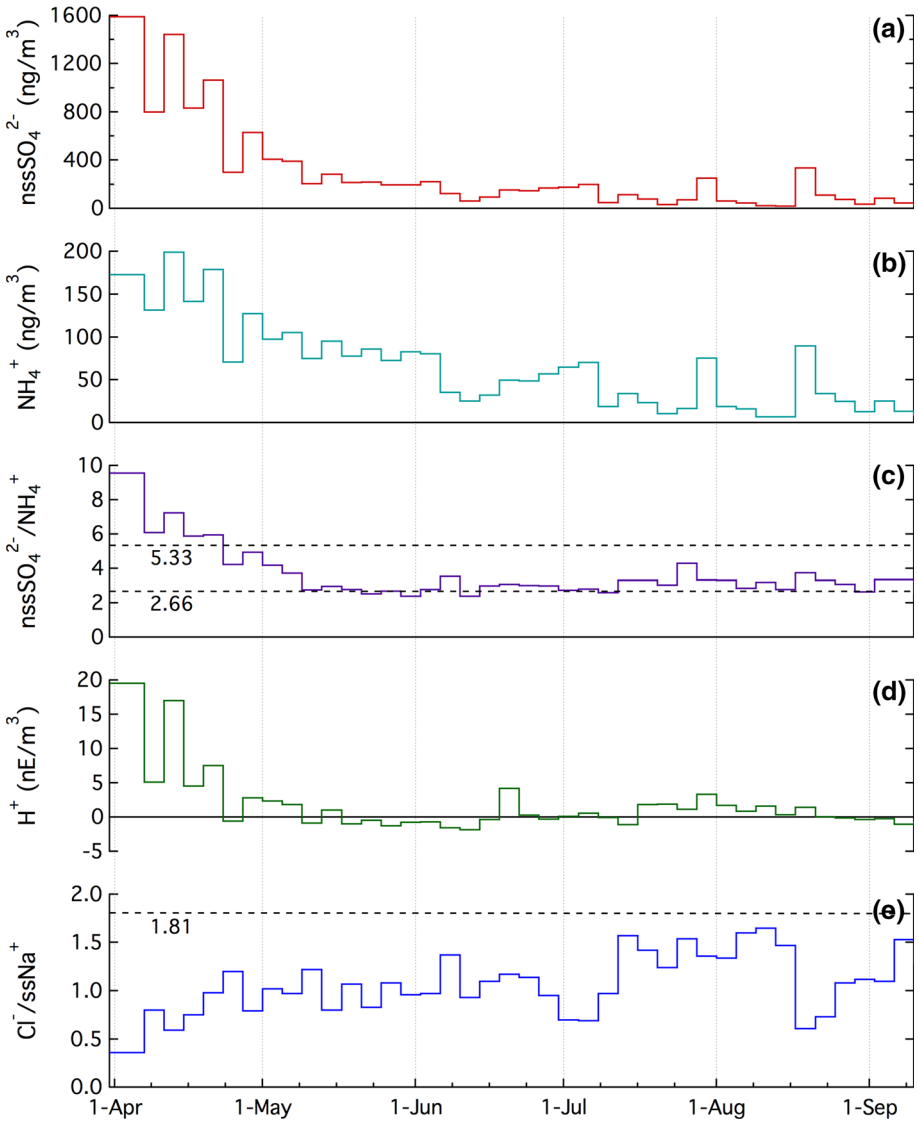

Fig. 5 Temporal profiles of: $nssSO_4^{2-}$ (**a**), NH_4^+ (**b**), $nssSO_4^{2-}/NH_4^+$ ratio (**c**), H^+ (**d**), and $Cl^-/ssNa^+$ ratio (**e**) in the sub-micrometric aerosol fraction

homogeneous and heterogeneous phase) of dimethylsulfide (DMS), in turn emitted by phytoplanktonic metabolic processes (e.g., Saltzmann 1995).

The other component arising from dimethylsulfide oxidation is sulfate, which has other sources beside the biogenic emissions (see Udisti et al. 2016). The quantification of biogenic sulfate is difficult, because its ratio with MSA is not constant, but depends on latitude, temperature, irradiation intensity, and oxidant concentrations, which promotes the formation of SO_4^{2-} instead of MSA (Bates et al. 1992; Lundén et al. 2007; Gondwe et al. 2003, 2004).

The seasonal pattern of MSA in the PM_{10} at Gruvebadet and Zeppelin Station located few hundred meters away at 470 m a.s.l. (Sharma et al. 2012), present a similar trend with maximum values in May–June, but the concentration levels in the two sites are quite different with concentration at Zeppelin higher than Gruvebadet. These differences can be due to the different time period considered: 1998–2010 for Zeppelin (Sharma et al. 2012) and 2013 in this work, but more likely to the boundary layer dynamic. The strong vertical stratification can restrict the transport of particulate MSA from the free troposphere, where it is formed by the oxidation of gaseous DMS, to the Arctic boundary layer (ABL). Since the Zeppelin site is located over the ABL, it is more affected than Gruvebadet by the transport from the marine source areas to Ny-Ålesund of aerosol containing MSA.

Regarding the size distribution, as observed for $nssSO_4^{2-}$, MSA was mainly distributed in the sub-micrometric fraction (Table 4; Fig. 7), suggesting that the preferred oxidation path is the photo-chemical oxidation occurring in gas phase, followed by gas to particle conversion. An oxidation in heterogeneous phase on sea salt particles would have led to higher concentrations in the

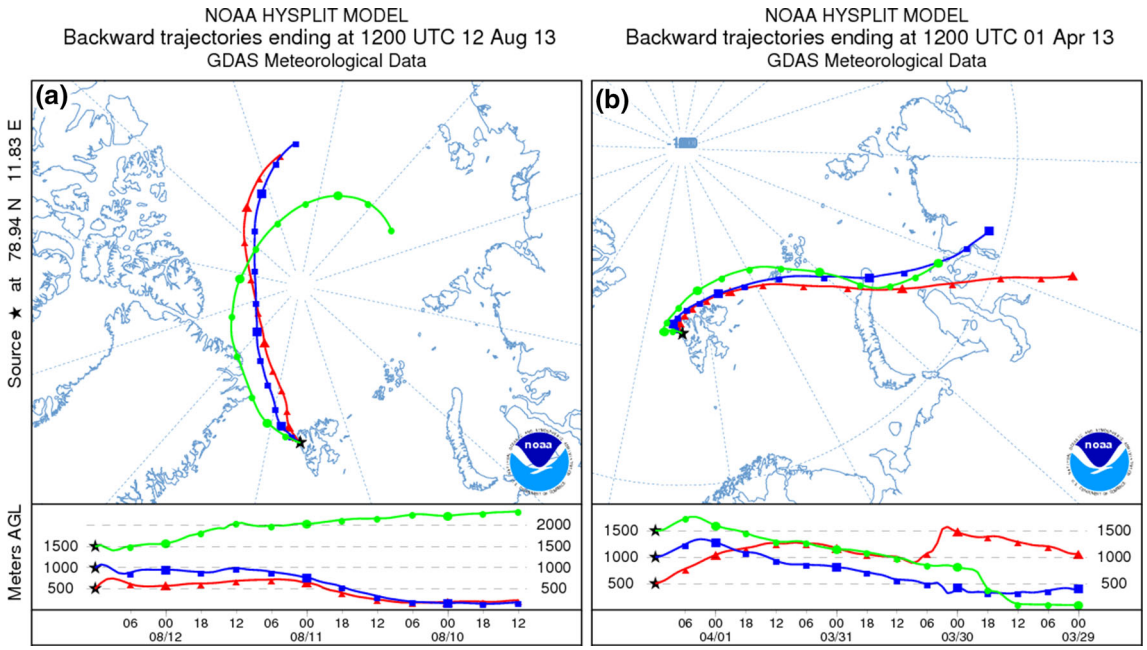

Fig. 6 Comparison between backtrajectories (72 h) in days of **a** no chloride depletion and **b** high chloride depletion

super-micrometric stages, where the sea spray particle is mainly present, as observed in early summer in Antarctica (Becagli et al. 2012).

The temporal trend of MSA in the sub-micrometric stage (Fig. 7) shows the highest concentrations from the end of April to early June, with maxima in mid-May, when values as high as 80 ng/m^3 were occasionally measured. Such summer maximum contemporaneously occurs with the peak of sea ice melting and can be related to the biogenic productivity at the marginal ice zone in the surrounding oceanic areas (Becagli et al. 2016).

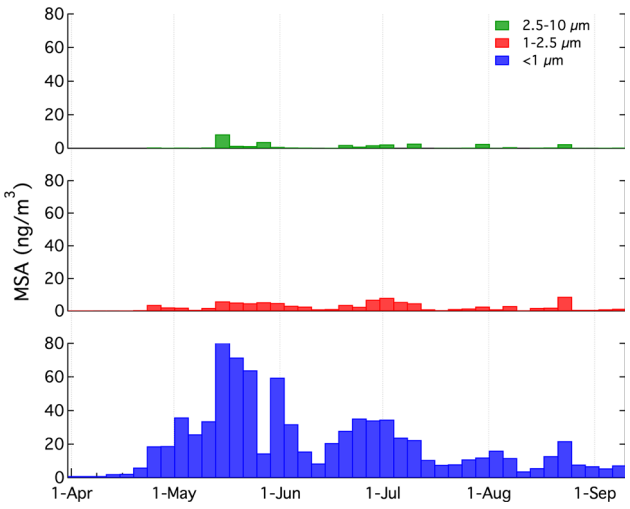

Fig. 7 Temporal trend of MSA in three size stages

4 Conclusions

During the spring–summer 2013 Italian Arctic campaign, particle size-distribution measurements and aerosol sampling for chemical analysis were carried out.

Particle counts in the range 0.01–20 μm showed a different pattern in early spring, with respect to the rest of the campaign. The first step was characterized by the dominance of particles in the accumulation mode (0.2–0.8 μm), probably due to anthropic nssSO_4^{2-} in the Arctic Haze. Successively, particle population shifted toward lower size ranges. In late spring–summer period, the main size mode was around 35 nm, and 50 events of NPF are evident in the period late April–August. The high occurrence of NPF events can be considered the result of both photochemical production of nucleating/condensing species and low condensation sink.

PM_{10} was collected at daily resolution, while a multistage impactor with 4-day resolution was used to obtain the aerosol size distribution in the ranges: <1.0 μm, 1.0–2.5, 2.5–10 μm, and >10 μm. Samples were analyzed by ion chromatography, and results were discussed to identify and quantify the contribution of the main sources: sea spray, long-range anthropic sulfates, and biogenic emissions.

ssNa^+, as univocal marker of sea spray, was used to calculate the sea salt contribution of Cl^-, SO_4^{2-}, Mg^{2+}, Ca^{2+}, and K^+. The size distribution of ssNa^+ shows that sea spray particles are mostly distributed in the 1.0–10 μm range.

Sulfate was the dominant species in the Ny-Ålesund aerosol and was mostly distributed in the sub-micrometric range, confirming that secondary sources (from atmospheric oxidation of SO_2) were dominant with respect to primary emissions from sea spray and crustal scraping. Non-sea salt sulfate was considered as a reliable marker of anthropic sources, especially in spring, when the biogenic contribution is low. $NssSO_4^{2-}$ was long-range transported from lower-latitude industrialized areas, and its acidic form (H_2SO_4) was the most probable agent for chloride removal (as HCl) in aged sea-spray particles. The chloride depletion, with respect to seawater composition, was particularly evident in the sub-micrometric fraction and in spring, when H_2SO_4 was not completely neutralized by ammonia and free acidity was available. Indeed, the $nssSO_4^{2-}/NH_4^+$ w/w ratio shows early-spring values higher than 5.33, corresponding to NH_4HSO_4 formation. On the other hand, summer values were consistently around 2.66, the ratio value corresponding to the complete neutralization of H_2SO_4 with ammonia to give $(NH_4)_2SO_4$.

MSA, mainly distributed in the sub-micrometric fraction, was used as univocal biogenic marker. Its temporal trend suggested the occurrence of two periods in which the phytoplanktonic activity was intense, with maximum values in late April–July.

Acknowledgements This peer-reviewed article is a result of the multi and interdisciplinary research activities based at the Arctic Station "Dirigibile Italia", coordinated by the "Dipartimento Scienze del Sistema Terra e Tecnologie per l'Ambiente" of the National Council of Research. This study was partially funded by the Italian Ministry of University and Research (MIUR) within the framework of the PRIN-2007 ("Dirigibile Italia") and PRIN-2009 ("Arctica") projects. The logistic assistance of the Polar Support Unit of the CNR Department of Earth and Environment (POLARNET) is gratefully acknowledged. This work was also partially supported by Italian MAE (Ministry of Foreign Affairs), within a bilateral cooperation program, in the framework of the Italy-South Korea agreement 2013-2015. The authors gratefully acknowledge the NOAA Air Resources Laboratory (ARL) for the provision of the HYSPLIT transport and dispersion model used in this publication.

References

Albrecht BA (1989) Aerosols, cloud microphysics and fractional cloudiness. Science 245:1227–1230

Bates TS, Calhoun JA, Quinn PK (1992) Variations in the methanesulfonate to sulfate molar ratio in submicrometer marine aerosol particles over the South Pacific Ocean. J Geophys Res 97:9859–9865

Bazzano A, Ardini F, Grotti M, Malandrino M et al (2016) Elemental and lead isotopic composition of atmospheric particulate measured in the Arctic region (Ny-Ålesund, Svalbard Islands). Rend Fis Acc Lincei (this issue)

Becagli S, Scarchilli C, Traversi R, Dayan U, Severi M, Frosini D, Vitale V, Mazzola M, Lupi A, Nava S, Udisti R (2012) Study of present-day sources and transport processes affecting oxidised sulphur compounds in atmospheric aerosols at Dome C (Antarctica) from year-round sampling campaigns. Atmos Environ 52:98–108

Becagli S, Lazzara L, Marchese C, Dayan U, Ascanius SE, Cacciani M, Caiazzo L, Di Biagio C, Di Iorio T, Di Sarra A, Eriksen P, Fani F, Giardi F, Meloni D, Muscari G, Pace G, Severi M, Traversi R, Udisti R (2016) Relationships linking primary production, sea ice melting, and biogenic aerosol in the Arctic. Submitted to Atmospheric Environment

Bowen HJM (1979) Environmental Chemistry of the Elements. Academic Press

Dal Maso M, Kulmala M, Riipinen I, Wagner R, Hussein T, Aalto PP, Lehtinen KEJ (2005) Formation and growth of fresh atmospheric aerosols: eight years of aerosol size distribution data from SMEAR II. Boreal Environ Res 10:323–336

Das R, Das SN, Misra VN (2005) Chemical composition of rainwater and dustfall at Bhubaneswar in the east coast of India. Atmos Environ 39:5908–5916

Engvall AC, Krejci R, Ström J, Treffeisen R, Scheele R, Hermansen O, Paatero J (2007) Changes in aerosol properties during spring-summer period in the Arctic troposphere. Atmos Chem Phys Discuss 7:1215–1260

Fisher JA, Jacob DJ, Wang Q, Bahreini R, Carouge CC, Cubison MJ, Dibb JE, Diehl T, Jimenez JL, Leibensperger EM, Lu Z, Meinders MBJ, Havala Pye OT, Quinn PK, Sharma S, Streets DG, van Donkelaar A, Yantosca RM (2011) Sources, distribution, and acidity of sulfate-ammonium aerosol in the Arctic in winter-spring. Atmos Environ 45:7301–7318

Gondwe M, Krol M, Gieskes W, Klaassen W, de Baar H (2003) The contribution of ocean-leaving DMS to the global atmospheric burdens of DMS, MSA, SO_2, and NSS SO_4^{2-}. Global Biogeochemical Cycles 17(2):1056

Gondwe M, Krol M, Klaassen W, Gieskes W, de Baar H (2004) Comparison of modeled versus measured MSA:nss SO_4^{2-} ratios: a global analysis. Global Biogeochemical Cycles 18, GB2006

Heintzenberg J, Hansson HC, Lannefors H (1981) The chemical composition of arctic haze at Ny-Alesund, Spitsbergen. Tellus 33:162–171

Henderson P, Henderson GM (2009) The Cambridge handbook of earth science data. Cambridge University Press

IPCC 2014, Kirtman B, Power SB, Adedoyin JA, Boer GJ, Bojariu R, Camilloni I, Doblas-Reyes FJ, Fiore AM, Kimoto M, Meehl GA, Prather M, Sarr A, Schär C, Sutton, R, van Oldenborgh GJ, Vecchi G, Wang HJ (2013) Near-term Climate Change: Projections and Predictability. In: Climate Change 2013: The Physical Science Basis. Contribution of Working Group I to the Fifth Assessment Report of the Intergovernmental Panel on Climate Change. Cambridge University Press, Cambridge, United Kingdom and New York, NY, USA

Iversen T, Joranger E (1985) Arctic air-pollution and large scale atmospheric flows. Atmos Environ 19:2099–2108

Kulshrestha UC, Sarkar AK, Srivastava SS, Parashar DC (1996) Investigation into atmospheric deposition through precipitation studies at New Delhi (India). Atmos Environ 30:4149–4154

Leck C, Persson C (1996) Seasonal and shot-term variability in dimethyl sulfide, sulfur dioxide and biogenic sulfur and sea salt aerosol particles in the arctic marine boundary layer during summer and autumn. Tellus 48B:272–299

Lundén J, Svensson G, Leck C (2007) Influence of meteorological processes on the spatial and temporal variability of atmospheric dimethyl sulfide in the high Arctic summer. J Geophys Res 112:D13308

Pincus R, Baker M (1994) Precipitation, solar absorption, and albedo susceptibility in marine boundary layer clouds. Nature 372:250–252

Quinn PK, Shaw G, Andrews E, Dutton EG, Ruoho-Airola T, Gong SL (2007) Arctic haze: current trends and knowledge gaps. Tellus 59:99–114

Robock A (1983) Ice and snow feedbacks and the latitudinal and seasonal distribution of climate sensitivity. J Atmos Sci 40:986–997

Röthlisberger R, Mulvaney R, Wolff EW, Hutterli MA, Bigler M, Sommer S, Jouzel J (2002) Dust and sea salt variability in central East Antarctica (Dome C) over the last 45 kyrs and its implications for southern high-latitude climate. Geophys Res Lett 29:1963

Saltzman ES (1995) Ocean/atmosphere cycling of dimethylsulfide. In: Delmas RJ, ed. Ice-core Studies of Global Biogeochemical Cycle. Berlin, etc., Springer-Verlag, 65-89. (NATO ASI Series I: Global Environmental Change, 30)

Screen JA, Simmonds I (2010) The central role of diminishing sea ice in recent Arctic temperature amplification. Nature 464:1334–1337

Sharma S, Chan E, Ishizawa M, Toom-Sauntry D, Gong SL, Li SM, Tarasick DW, Leaitch WR, Norman A, Quinn PK, Bates TS, Levasseur M, Barrie LA, Maenhaut W (2012) Influence of transport and ocean ice extent on biogenic aerosol sulfur in the Arctic atmosphere. J Geophys Res 117:D12209

Shaw GE (1984) Microparticle size spectrum of Arctic haze. Geophys Res Lett 11:409–412

Stein AF, Draxler RR, Rolph GD, Stunder BJB, Cohen MD, Ngan F (2015) NOAA's HYSPLIT atmospheric transport and dispersion modeling system. Bull Am Meteorol Soc 96:2059–2077

Ström J, Umegård J, Tørseth K, Tunved P, Hansson HC, Holmén K, König-Langlo G (2003) One year of particle size distribution and aerosol chemical composition measurements at the Zeppelin Station, Svalbard, March 2000-March 2001. Phys Chem Earth 28:1181–1190

Tunved P, Ström J, Krejci R (2013) Arctic aerosol life cycle: linking aerosol size distributions observed between 2000 and 2010 with air mass transport and precipitation at Zeppelin station, Ny-Ålesund, Svalbard. Atmos Chem Phys 13:3643–3660

Udisti R, Dayan U, Becagli S, Busetto M, Frosini D, Legrand M, Lucarelli F, Preunkert S, Severi M, Traversi R, Vitale V (2012) Sea spray aerosol in central Antarctica. Present atmospheric behaviour and implications for paleoclimatic reconstructions. Atmos Environ 52:109–120

Udisti R, Bazzano A, Becagli S, Bolzacchini E et al (2016) Sulfate source apportionment in the Ny-Ålesund (Svalbard Islands) Arctic aerosol. Rend Fis Acc Lincei (this issue)